Research Article Vol. 33, No. 11 / 2 Jun 2025 / Optics Express 23244
Optics EXPRESS

Light sensor based on carbon tetrachloride-infiltrated side-hole fiber

YUBIN DENG,[1,2] YING WANG,[1,2,*] HAN LIU,[1,2] YUNFANG ZHANG,[1,2] CHANGRUI LIAO,[1,2] DEJUN LIU,[1,2] AND YIPING WANG[1,2]

[1]*Shenzhen Key Laboratory of Ultrafast Laser Micro/Nano Manufacturing, Key Laboratory of Optoelectronic Devices and Systems of Ministry of Education/Guangdong Province, College of Physics and Optoelectronic Engineering, Shenzhen University, Shenzhen 518060, China*
[2]*Shenzhen Key Laboratory of Photonic Devices and Sensing Systems for Internet of Things, Guangdong and Hong Kong Joint Research Centre for Optical Fibre Sensors, State Key Laboratory of Radio Frequency Heterogeneous Integration, Shenzhen University, Shenzhen 518060, China*
[*]*yingwang@szu.edu.cn*

Abstract: We propose a high-sensitivity light sensor based on side-hole optical fiber filled with carbon tetrachloride. Using a fusion splicer, we employed a selective glue coating method to fill one of the air holes with liquid. Coupling occurs between the propagation modes of the liquid waveguide filled with carbon tetrachloride and the core propagation modes, resulting in resonant dips in the transmission spectrum. When the temperature changes, the refractive index of carbon tetrachloride changes, affecting the coupling and causing the wavelength of resonant dips to shift. In this experiment, the temperature sensitivity of the sensor was tested and reached up to 46 nm/°C. Utilizing its high-temperature sensitivity, the infrared laser light intensity was measured with a sensitivity of 0.114 nm/(mW/cm^2). While maintaining a high level of sensitivity, the sensor is also easy to fabricate and cost-effective. Therefore, it holds great potential for applications requiring high-precision laser power measurement, laser manipulation, optical modulation, and optical switching.

1. Introduction

Side-hole optical fiber (SHF) is a new type of microstructure optical fiber. It features two symmetric air holes adjacent to the fiber core along the fiber axis within its cladding. The structure of SHF is similar to that of panda polarization-maintaining fibers, but differs in that the two holes next to the core are hollow. SHF is first proposed and studied in 1986 [1]. Due to its unique structure, it can be made into a variety of optical fiber sensors, such as Sagnac interferometers, Mach-Zehnder interferometers, Michelson interferometers, mode-coupling types, long-period grating types, Bragg grating types, and Fabry-Pérot interferometers. Due to their unique structure, they are widely used for measurements of pressure [2–4], temperature [5–7], strain [8], humidity [9], refractive index [10,11], and electric and magnetic fields. In 2013, a SHF Sagnac ring interferometer filled with alcohol was proposed [5]. By detecting the drift of the Sagnac interference peak, a sensitivity of 86.8 pm/°C was achieved, which is higher than that of fiber Bragg grating sensors. In 2018, an ethanol-filled SHF sensor based on Mach-Zehnder interferometer theory was proposed [6]. By splicing the ethanol-filled SHF at one end of two single-mode fibers, interference between the core and cladding modes was excited. The measured temperature sensitivity reached 105 pm/°C by detecting the drift of the resonant peak in the transmission spectrum. In 2019, a liquid crystal-filled side-hole optical fiber sensor based on mode-coupling theory was proposed [7]. Liquid crystals were selectively filled into specific air hole, forming a waveguide coupling structure between the liquid crystal-filled waveguide and the core waveguide. The resonant peaks in the transmission spectrum were used for sensing,

#560044 https://doi.org/10.1364/OE.560044
Journal © 2025 Received 26 Feb 2025; revised 8 May 2025; accepted 8 May 2025; published 27 May 2025

Optics EXPRESS

achieving a temperature sensitivity of 1.5 nm/°C. Thus, it can be seen that temperature sensors based on SHF of different structures generally suffer from low sensitivity, with sensitivities typically ranging from one nm to tens of pm/°C.

Due to the advantages of optical fiber light sensors such as immunity to electromagnetic interference, simple structure, and high sensitivity, they have great application prospects in fields like optical modulation, optical switching, and laser manipulation. In 2010, a Bragg grating light sensor based on azobenzene coating was proposed. The wavelength of the grating peak shifted with changes in ultraviolet light intensity, with an average sensitivity of 0.00288 nm/(mW /cm^2) [12]. In 2011, a micro-optical fiber ring resonator with a photosensitive liquid crystal mixture was proposed. The refractive index changed with varying light intensity, causing a shift in the resonance wavelength, with a sensitivity of 0.003 nm/(mW/cm^2) [13]. In 2015, a Mach-Zehnder interferometer sensor for detecting light intensity was proposed. By combining the photosensitivity of an ethyl orange solution, the sensor measured the light power, achieving a resonance wavelength sensitivity of 0.02576 nm/(mW/cm^2) [14]. It can be seen that optical fiber light sensors generally face the problem of low sensitivity.

In response to these issues, we propose an ultra-high sensitivity optical fiber light sensor. In this study, we selectively filled a 1 cm section of SHF with carbon tetrachloride. Carbon tetrachloride (CCl_4) is a colorless, transparent liquid widely used as an organic solvent, dry-cleaning agent, and refrigerant [15]. It has a large thermo-optic coefficient [16,17] and shows significant absorption in the infrared region [18]. The refractive index at a wavelength of 1550 nm is 1.4474 [19], and its thermo-optic coefficient is -4.0 $\times$ 10^{-4}/°C. The sensor essentially functions as a directional coupler between the fiber core waveguide and the carbon tetrachloride-filled liquid waveguide. When phase matching conditions are met [20], light at specific wavelengths transmitted through the fiber core will couple into the liquid waveguide, forming multiple resonant peaks. Sensing is achieved by detecting the wavelength change of the resonant peak. In experiments, a temperature sensitivity of up to 46 nm/°C was achieved. Due to the similar slopes of the dispersion curves of the liquid mode filled with carbon tetrachloride and the core fundamental mode, the sensor exhibits high sensitivity. Using this high temperature sensitivity, light intensity can be measured, with a light intensity sensitivity of up to 0.114 nm/(mW/cm^2). Compared to previous optical fiber light sensors, the sensitivity is significantly improved, and it requires only a simple glue filling process. This results in a high sensitivity, simple structure, easy fabrication, and low cost advantage.

2. Sensor fabrication

The SHF used in the experiment consists of two air holes adjacent to the fiber core. The distance from the fiber core center to the air hole is 26 μm, and the diameter of the air holes is 36 μm. The diameters of the cladding and core are the same as those of standard single-mode fibers. Using a splicer and ultraviolet light (UV) glue, we selectively sealed one of the air holes.

First, the side-hole fiber with a properly cut end face and the single-mode fiber (SMF) with a small amount of UV glue applied were placed into the splicer, as shown in Fig. 1(a). The SHF was rotated so that the direction of the two air holes aligned parallel to the field of view. Then, by manually controlling the splicer motor, the SHF and the SMF coated with a small amount of UV glue were misaligned. The offset distance was approximately 26 μm. The SMF was moved to contact the selected air hole, and then quickly moved away to prevent excessive glue from flowing into the other air hole. Finally, the UV glue was solidified using a UV lamp, effectively sealing one of the air holes.

The end face of the fiber with one air hole selectively sealed is shown in Fig. 1(b). The upper hole, filled with UV glue and exposed to light, appears bright, while the lower hole remains dark. The end face of the SHF with the UV glue was inserted into a beaker containing CCl_4 and left undisturbed for 10 minutes. Due to capillary action, the CCl_4 filled the entire fiber. The process

Optics EXPRESS

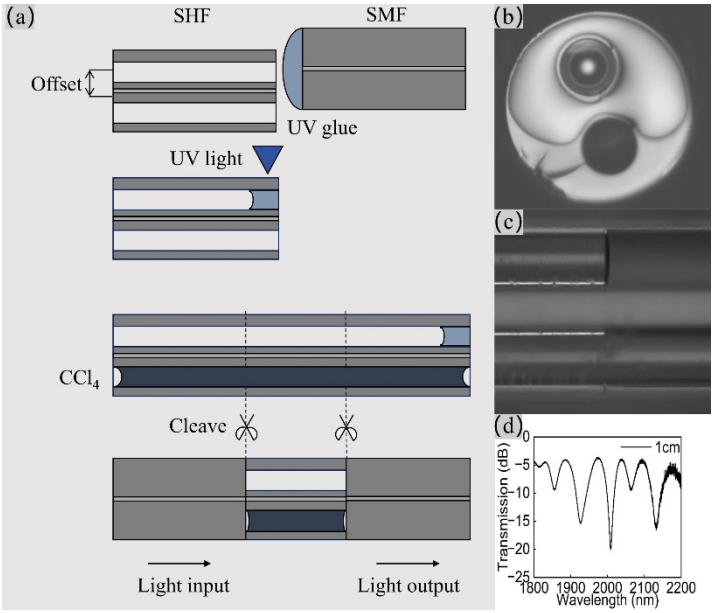

Fig. 1. (a) Illustration of the device fabrication procedures, where simple glue coating, UV curing, CCl4 filling, fiber cleaving and fusion splicing are included. (b) The end-face image of the glue coated SHF. (c) The microscopic image of the SHF after CCl4 filling in side view. (d) Typical transmission spectrum of a 1 cm-long device.

is simple and fast. The SHF selectively filled with is CCl_4 shown in Fig. 1(c). It is evident that one of the air holes is filled with CCl_4, while the other remains unfilled.

The CCl4 used in this study was bought from the Rhawn Company. To achieve deeper resonant dips and lower loss, we cleave the SHF by using a homemade precision fiber cleaver with a microscope system. Then the SHF is connected to SMF at both ends. The SMF fiber ends were connected to a light source (YSL, SC-5) and an optical spectrum analyzer (Yokogawa, AQ6375B) to observe the transmission spectrum. The optical spectrum analyzer can detect light at wavelengths of 1200-2400 The light source and the optical spectrum analyzer detected the transmission spectrum as shown in Fig. 1(d). Within the wavelength range of 1800–2200 nm, five resonant dips were observed. The spectral fluctuations near the longer wavelengths were caused by the instability of the light source. The resonant peaks appeared because the multimode liquid waveguide formed by the CCl_4 and the core waveguide together created a waveguide coupling structure. When light propagates through the fiber core, some modes with specific wavelengths couple into the liquid waveguide, leading to the appearance of multiple resonant dips in the spectrum as shown in Fig. 1(d).

Figure 2 shows the transmission spectrum evolution for the sensor length changing from 0.7 to 1.4 cm, where the black curve shows the case without liquid filling. Experimental results indicate that the sensor with a length of 1 cm exhibits the highest extinction ratio. The positions of the dips and the distance between the dips are approximately the same. Therefore, a sensor length of 1 cm was chosen.

3. Sensing experiments and discussions

We placed the approximately 1 cm-long device into a temperature furnace (Ecom, LCO102), which can adjust the temperature from room temperature to 100°C with a precision of 0.1°C. The

Optics EXPRESS

device was stretched and secured inside the furnace using adhesive tape to prevent strain-induced interference.

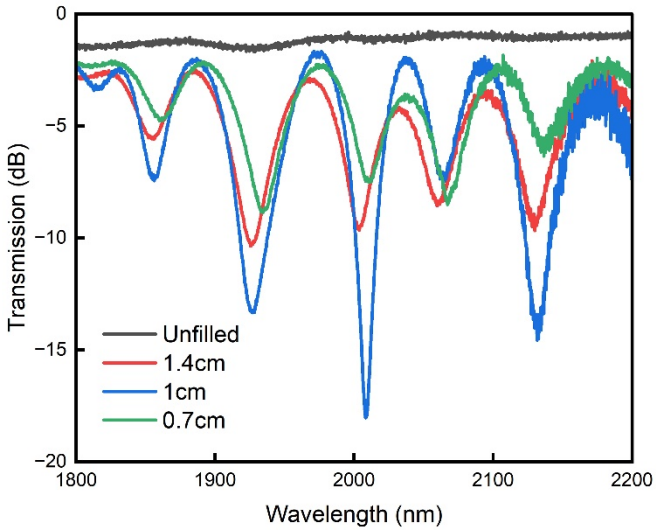

Fig. 2. Transmission spectra of the proposed light sensors with different SHF lengths.

The temperature of the furnace was set to vary from 25°C to 30°C, and a set of data was collected. It can be observed that the resonant wavelength of the device exhibits a redshift as the temperature increases, which will be explained theoretically later. Figure 3(a) shows the spectrum evolution of the device as temperature changes within a free spectral range. The first resonant wavelength in shorter wavelength direction is plotted in Fig. 3(b) with temperature increasing, where an average temperature sensitivity of 46 nm/°C can be obtained through linear fitting.

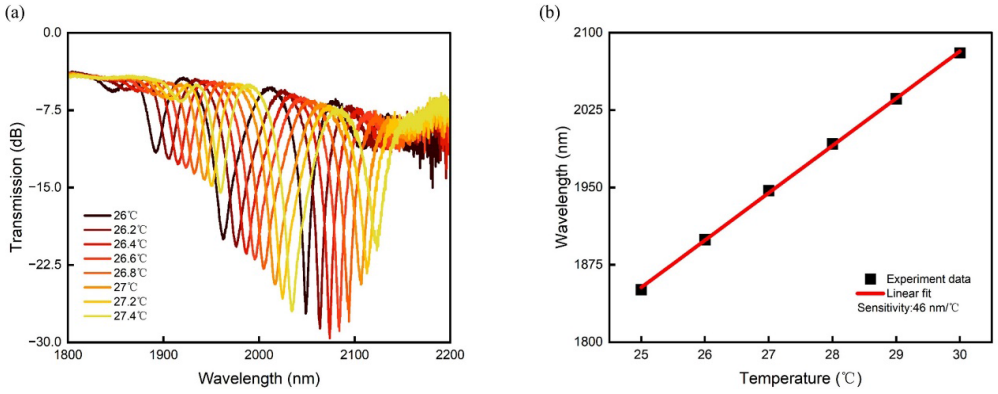

Fig. 3. (a) The transmission spectrum evolution of the device with temperature increasing. (b) Relationship between the resonant wavelength and temperature.

The standard mode coupling theory of directional couplers can effectively explain the appearance of resonant dips. In our experiment, the resonant dips are attributed to the coupling between the fundamental core mode and the liquid waveguide mode.

To further verify the operating principle and temperature sensitivity of the SHF filled with CCl_4, we established a model in the simulation software COMSOL Multiphysics based on the

Optics EXPRESS

fiber's geometric structure and material refractive indices using the finite element method. This allowed us to analyze the coupling characteristics of the fiber modes. During the simulation, we approximated degenerate mode dispersion curves within the same group as a single curve due to their similarity. In the calculations, we considered the material dispersion curves of both CCl_4 and fused silica.

Figure 4(a) illustrates the dispersion curves of the solid core fundamental mode and various liquid waveguide modes supported by the CCl_4-filled waveguide. Mode coupling occurs when the effective refractive indices of the core fundamental mode and the liquid waveguide modes are equal [21]. From Fig. 4(a), five intersection points are observed between the core mode and the liquid waveguide modes, indicating the presence of five resonant dips, which correspond well to the experimental results shown in Fig. 1(d).

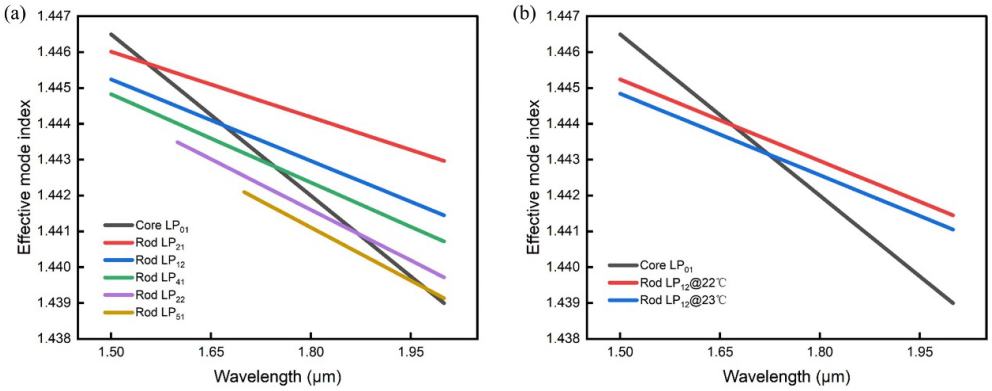

Fig. 4. (a) The dispersion curves of different modes in the liquid-filled waveguide and the core fundamental mode. (b) Dispersion curves of the fiber core mode and the Rod LP_{12} mode at temperatures of 22°C and 23°C, respectively, which clearly indicates the temperature effect on the resonant wavelength.

It is worth noting that deviations in the refractive indices of materials or the geometric parameters of the fiber in the simulations can lead to significant discrepancies between the simulated and experimentally observed coupling wavelengths. We selected the liquid mode LP_{12} for temperature simulations. Due to the similar slopes of the dispersion curves for multiple liquid waveguide modes and the unchanging slope of the core mode dispersion curve, the temperature sensitivities of the modes are approximately the same. Thus, we focused on the LP_{12} mode for temperature simulation.

The CCl_4 used in our experiment has a negative thermo-optic coefficient, which is 2 orders of magnitude higher than that of silica. Therefore, we neglected the effect of temperature changes on the core fundamental mode. Figure 4(b) shows the dispersion curves of the core fundamental mode and the liquid LP_{12} mode at 22°C and 23°C, respectively. When the temperature increases, the refractive index of the LP_{12} mode decreases, causing its dispersion curve to shift downward. This results in the resonant wavelength shifting toward longer wavelengths. The temperature sensitivity of the simulation is 53.91 nm/°C, which is in good agreement with the temperature sensitivity of 46 nm/°C tested in the experiment. Through simulation, it is found that the dispersion curves of the higher order core modes are much lower than that of the fundamental core mode, and no coupling can be observed between these modes and the liquid mode within the observable range. Therefore, only the fundamental core mode is considered for the sensor design.

To explore further applications using the high-temperature sensitivity of this device, we conducted additional investigations. CCl_4 is an excellent photothermal material with significant absorption effects in the infrared region. We measured the absorption spectrum of CCl_4 using

Optics EXPRESS

a UV-Vis spectrophotometer, as shown in Fig. 5(a). The principle is based on the absorption spectrum generated by the transitions of outer valence electrons in molecules [22]. As seen in the figure, CCl_4 exhibits a relatively flat curve in the wavelength range of 400–1100 nm, indicating consistent absorption across this range.

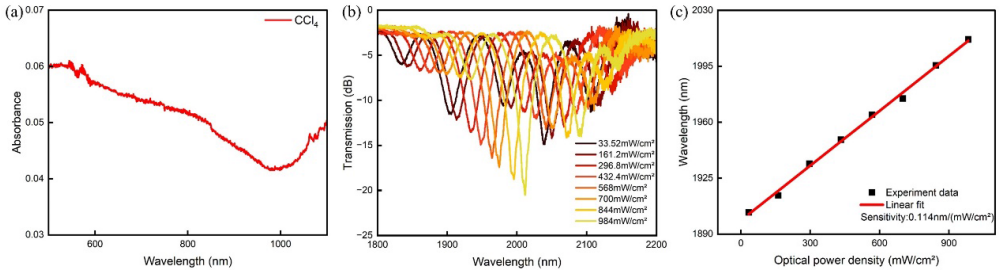

Fig. 5. (a) The absorption spectrum of CCl_4. (b) The transmission spectrum of the proposed device under different laser power levels. (c) Relationship between the resonant wavelength and 1030-nm laser intensity.

We used an infrared laser with a central wavelength of 1030 nm and a repetition rate of 1 MHz to irradiate the device. The output beam had a diameter of 0.5 cm. One end of the device was connected to the light source, and the other end was connected to an optical spectrum analyzer to monitor spectral changes in real time, as shown in Fig. 5(a).

When CCl_4 absorbs infrared light, it converts the light energy into thermal energy, causing a temperature rise and resulting in a redshift of the resonant dips wavelength. It is important to maintain a constant ambient temperature during the experiment to minimize environmental influence due to the high-temperature sensitivity of the device.

In the experiment, the applied light density ranged from 33.52 mW/cm^2 to 984 mW/cm^2. The resonant dips shifted toward longer wavelengths and we selected a resonant dip at around 1900nm for linear fitting with the light density. The total redshift was 109.4 nm, as shown in Fig. 5(c), resulting in a laser power sensitivity of 0.114 nm/(mW/cm^2).

The detection limit of the device can be calculated using the sensitivity and resolution [23,24]:

$$DL = R/S \tag{1}$$

$$R = 3\sqrt{\sigma^2_{ampl-noise} + \sigma^2_{temp-induced} + \sigma^2_{spect-res}} \tag{2}$$

R represents the resolution of the sensor. S represents the sensitivity of the sensor. $\Delta\lambda$ represents the full-width-half-max of the mode amplitude (FWHM). The FWHM of the resonant dips is about 30 nm. The resolution of the spectrometer we set is 1 nm. $\sigma^2_{ampl-noise}=\Delta\lambda/4.5(SNR^{0.25}) = 0.21$ nm. We assume that the SNR is 60 dB and the value of $\sigma^2_{temp-induced}$ is 8fm. Assuming that the position error of the resonant dips is uniformly distributed from -0.5 nm to 0.5 nm, we can calculate the value of $\sigma^2_{spect-res}$ is 0.29 nm. Therefore, we can theoretically calculate R = 1.08 nm, DL = R/S = 9.474 mW/cm^2.

The detection limit of the proposed light sensor can also be evaluated by detecting the fluctuation of wavelength. Without environmental perturbation, the sensor was exposed to light with an intensity of 161.2 mW/cm^2. Spectral data were collected at two second intervals, as shown in Fig. 6. The resonance wavelength exhibited small fluctuations, indicating good stability of the device. In the experiment, the calculated standard deviation (σ) is 0.63 nm. With R = 3σ=1.89 nm, the DL can be estimated to be 16.57 mW/cm^2 according to Eq. (1), which is larger than that of the theoretical one. This is possibly caused by the perturbation of environmental temperature fluctuation.

Optics EXPRESS

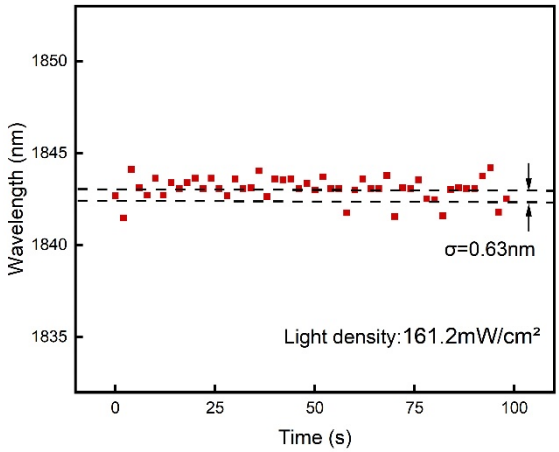

Fig. 6. Resonant wavelength fluctuation under1030-nm laser irradiation with a light intensity of 161.2 mW/cm^2.

4. Conclusion

We propose an ultra-high sensitivity light sensor based on CCl_4-filled SHF, which offers advantages such as low cost, simple fabrication process, and straightforward structure while maintaining high sensitivity. The operating principle of the device is based on the coupling between the fundamental mode of the core and the liquid mode of CCl_4. Due to the similarity in their dispersion curves, the sensitivity of the sensor is significantly enhanced. In our experiments, the measured temperature sensitivity was 46 nm/°C. Leveraging its high-temperature sensitivity, the device was used to measure light intensity, achieving a sensitivity of 0.114 nm/(mW/cm^2). These advantages make it highly promising for applications requiring optical modulation, optical switching, and laser manipulation.

Funding. National Key Research and Development Program of China (2024YFB3213700); National Natural Science Foundation of China (62475170); Natural Science Foundation of Guangdong Province (2023A1515012893); Science and Technology Innovation Commission of Shenzhen (JCYJ20220818095615034); Shenzhen Key Laboratory of Ultrafast Laser Micro/Nano Manufacturing (ZDSYS20220606100405013).

Disclosures. The authors declare no conflicts of interest.

Data availability. Data underlying the results presented in this paper are not publicly available at this time but may be obtained from the authors upon reasonable request.

References

1. H. M. Xie, K. Okamoto, Ph. Dabkiewicz, *et al.*, "Side-hole fiber for fiber-optic pressure sensing," Opt. Lett. **11**(5), 333 (1986).
2. Z. Yang, W. Yuan, Y. Wang, *et al.*, "Compact Hybrid Interferometer Based on Twin- Core Side Hole Fiber and Harmonic Vernier Effect for Gas Pressure Measurement," IEEE Sensors J. **24**(5), 6173–6180 (2024).
3. J. R. Clowes, S. Syngellakis, and M. N. Zervas, "Pressure sensitivity of side-hole optical fiber sensors," IEEE Photonics Technol. Lett. **10**(6), 857–859 (1998).
4. W. J. Bock, M. S. Nawrocka, and W. Urbanczyk, "Highly sensitive fiber-optic sensor for dynamic pressure measurements," IEEE Trans. Instrum. Meas. **50**(5), 1085–1088 (2001).
5. Y. Xin, X. Dong, Q. Meng, *et al.*, "Alcohol-filled side-hole fiber Sagnac interferometer for temperature measurement," Sens. Actuators, A **193**, 182–185 (2013).
6. Y. Xin, M. Zhao, H. Zhao, *et al.*, "Alcohol-filled side-hole fiber based Mach-Zehnder interferometer for temperature measurement," Opt. Fiber Technol. **46**, 72–76 (2018).
7. Y. Huang, Y. Wang, C. Mao, *et al.*, "Liquid-Crystal-Filled Side-hole Fiber for High-Sensitivity Temperature and Electric Field Measurement," Micromachines **10**(11), 761 (2019).
8. O. Frazão, S. O. Silva, J. M. Baptista, *et al.*, "Simultaneous measurement of multiparameters using a Sagnac interferometer with polarization maintaining side-hole fiber," Appl. Opt. **47**(27), 4841 (2008).

Optics EXPRESS

9. S. Wu, G. Yan, Z. Lian, *et al.*, "An open-cavity Fabry-Perot interferometer with PVA coating for simultaneous measurement of relative humidity and temperature," Sens. Actuators, B **225**, 50–56 (2016).
10. Y. X. Jin, C. C. Chan, Y. F. Zhang, *et al.*, "Mechanically induced long-period fiber grating in side-hole single-mode fiber for temperature and refractive sensing," Opt. Commun. **283**(7), 1303–1306 (2010).
11. G. Liu, D. Feng, M. Zhang, *et al.*, "Side-Hole Plastic Optical Fiber for Testing Liquid's Refractive Index," IEEE Sens. J. 1-1 (2014).
12. H.-K. Kim, W. Shin, and T.-J. Ahn, "UV Sensor Based on Photomechanically Functional Polymer-Coated FBG," IEEE Photonics Technol. Lett. **22**(19), 1404–1406 (2010).
13. Z. Chen, V. K. S. Hsiao, X. Li, *et al.*, "Optically tunable microfiber-knot resonator," Opt. Express **19**(15), 14217 (2011).
14. H. Liu, H. Zhang, Y. Miao, *et al.*, "A light-intensity-controlled microfiber-assisted Mach–Zehnder interferometer based on ethyl orange solution under 532 nm laser excitation," Sens. Actuators, B **216**, 229–234 (2015).
15. T. Chakraborty and S. N. Rai, "Depolarization ratio and correlation between the relative intensity data and the abundance ratio of various isotopes of liquid carbon tetrachloride at room temperature," Spectrochim. Acta, Part A **62**(1-3), 438–445 (2005).
16. J. D. Olson and F. H. Horne, "Direct determination of temperature dependence of refractive index of liquids," J. Chem. Phys. **58**(6), 2321–2325 (1973).
17. K. Moutzouris, M. Papamichael, S. C. Betsis, *et al.*, "Refractive, dispersive and thermo-optic properties of twelve organic solvents in the visible and near-infrared," Appl. Phys. B **116**(3), 617–622 (2014).
18. S. Kedenburg, M. Vieweg, T. Gissibl, *et al.*, "Linear refractive index and absorption measurements of nonlinear optical liquids in the visible and near-infrared spectral region," Opt. Mater. Express **2**(11), 1588 (2012).
19. M. N. Polyanskiy, "Refractiveindex.info database of optical constants," Sci. Data **11**(1), 94 (2024).
20. J. Laegsgaard, O. Bang, and A. Bjarklev, "Photonic crystal fiber design for broadband directional coupling," Opt. Lett. **29**(21), 2473 (2004).
21. M. Yang, D. N. Wang, Y. Wang, *et al.*, "Fiber in-line Mach–Zehnder interferometer constructed by selective infiltration of two air holes in photonic crystal fiber," Opt. Lett. **36**(5), 636 (2011).
22. R. A. Dobbs, R. H. Wise, and R. B. Dean, "The use of ultra-violet absorbance for monitoring the total organic carbon content of water and wastewater," Water Res. **6**(10), 1173–1180 (1972).
23. I. M. White and X. Fan, "On the performance quantification of resonant refractive index sensors," Opt. Express **16**(2), 1020 (2008).
24. M. R. Lee and P. M. Fauchet, "Two-dimensional silicon photonic crystal based biosensing platform for protein detection," Opt. Express **15**(8), 4530 (2007).